Application of the Mathematical Theory of Plasticity for Developing New Methods of Material Testing

1 Introduction

The further development of metallic materials demands the determination of characteristics for strength and ductility. Often the volume of metallurgically produced new material compositions is rather small and expensive, so that the use of standardized tension or compression tests is excluded. It is, therefore, desirable to develop new methods of materials testing allowing for relatively small specimens. Stimulated by a research project of the Max-Planck-Institut für Eisenforschung on the development of new intermetallic compounds for high temperature service, three new test methods have been developed, which will be described here in detail: the small-cup drawing test, the mantle compression test, and the ball compression test. In order to analyze the stresses and strains involved in these three deformation processes some of the current methods of the mathematical theory of plasticity have been used successfully.

2 Small-Cup Drawing Test

Conventional tension tests demand relatively long specimens. With increasing temperature there may be additional experimental difficulties of correct clamping. These problems can be overcome by use of the small-cup drawing test. Fig. 1 shows its basic principle. A small cup, having a stiff bottom and a stiff border in comparison to the cylindrical wall, is positioned into a recipient. With an inserted ram it is then deformed in the longitudinal direction, whereby only the wall is stretched plastically. The advantages are obvious: compact geometry of specimen, no clamping difficulties by reason of external pressure forces, possibility of common heating of tools and specimen for the purpose of isothermal testing.

For the practical use of this test the question is to be answered whether the longitudinal stress can be used as a measure for the yield strength in tension. The solution is given by the method of upper bound on deformation power. To establish a kinematically admissible velocity field in cylindrical coordinates r, ϑ, z, the following

O. S. Brüller et al. (eds.), *Advances in Continuum Mechanics*

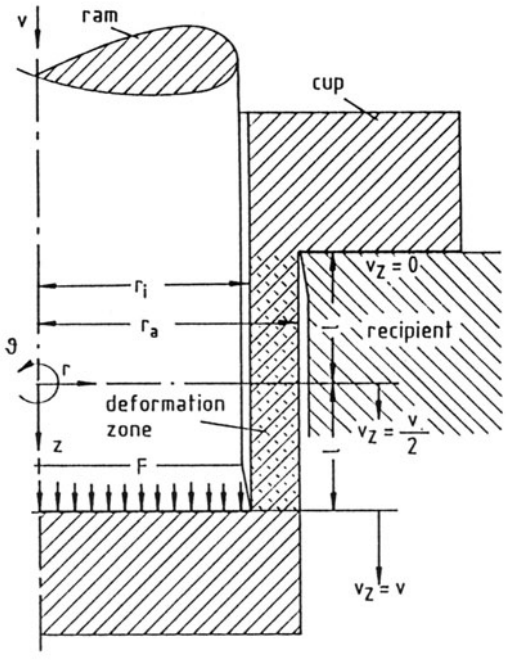

Fig. 1: Principle of the small-cup drawing test

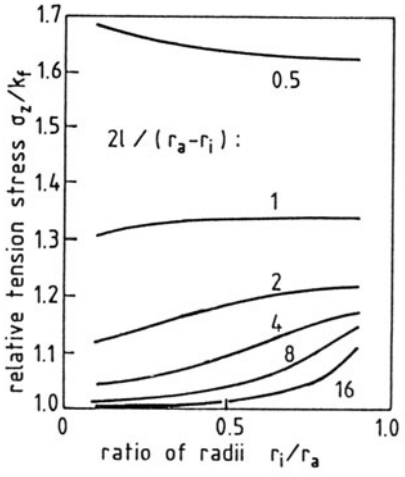

Fig. 2: Upper bound solution for the tension stress in the small-cup drawing test

assumptions are used

$$v_z = v_z(z), \tag{1}$$

$$v_r = f(r)g(z), \tag{2}$$

(v_z axial velocity, v_r radial velocity, f and g functions to be determined).

The condition of constant volume ($\dot{\epsilon}$ strain rate)

$$\dot{\epsilon}_r + \dot{\epsilon}_\vartheta + \dot{\epsilon}_z = \frac{\partial v_r}{\partial r} + \frac{v_r}{r} + \frac{\partial v_z}{\partial z} = 0 \tag{3}$$

gives

$$\frac{dv_z(z)}{dz} = - g(z)\left[\frac{df(r)}{dr} + \frac{f(r)}{r}\right], \tag{4}$$

from which

$$\frac{df(r)}{dr} + \frac{f(r)}{r} = \text{const.} = C \tag{5}$$

follows. The solution of this differential equation is

$$f(r) = \frac{r}{2}\left(C - \frac{1}{K^2 r^2}\right), \tag{6}$$

with K as an integration constant. If a neutral radius r_n is introduced by the condition

$$v_r(r_n) = 0\ , \tag{7}$$

it follows

$$K^2 = \frac{1}{C\, r_n^2}\ . \tag{8}$$

The radial velocity is then

$$v_r = \frac{C}{2} r \left(1 - \frac{r_n^2}{r^2}\right) g(z)\,. \tag{9}$$

For symmetry only positive values of z are considered. Then it is chosen (ℓ half length of deformation zone, p arbitrary exponent)

$$g(z) = \ell^p - z^p\,, \qquad 0 \le z \le \ell\,, \tag{10}$$

which satisfies the boundary condition $v_r = 0$ at $z = \ell$. Equations (4), (5), and (10) result in the differential equation for $v_z(z)$

$$\frac{dv_z(z)}{dz} = -C\,(\ell^p - z^p). \tag{11}$$

With the boundary conditions

$$v_z(0) = \frac{v}{2}, \qquad v_z(\ell) = v \tag{12}$$

(v speed of the ram) the velocity field is finally given by

$$v_z = \frac{v}{2p}\left[p + (p+1)\frac{z}{\ell} - \left(\frac{z}{\ell}\right)^{p+1}\right], \tag{13}$$

$$v_r = -v\,\frac{p+1}{4p}\,\frac{r}{\ell}\left[1 - \left(\frac{r_n}{r}\right)^2\right]\left[1 - \left(\frac{z}{\ell}\right)^p\right]. \tag{14}$$

This leads to the coordinates of the strain rate tensor $\dot{\epsilon}_{ij}$

$$\dot{\epsilon}_r = -\frac{v}{\ell}\,\frac{p+1}{4p}\left[1 + \left(\frac{r_n}{r}\right)^2\right]\left[1 - \left(\frac{z}{\ell}\right)^p\right], \tag{15}$$

$$\dot{\epsilon}_\vartheta = -\frac{v}{\ell}\,\frac{p+1}{4p}\left[1-\left(\frac{r_n}{r}\right)^2\right]\left[1-\left(\frac{z}{\ell}\right)^p\right], \tag{16}$$

$$\dot{\epsilon}_z = \frac{v}{\ell}\,\frac{p+1}{2p}\left[1-\left(\frac{z}{\ell}\right)^p\right], \tag{17}$$

$$\dot{\epsilon}_{rz} = \frac{v\,r}{\ell^2}\,\frac{p+1}{8}\left[1-\left(\frac{r_n}{r}\right)^2\right]\left(\frac{z}{\ell}\right)^{p-1}. \tag{18}$$

The deformation power L is to be minimized (F drawing force, k_f tension yield strength, V volume of deformation zone)

$$L = F\,v = \sqrt{\tfrac{2}{3}}\,k_f \int_V \sqrt{\dot{\epsilon}_{ij}\,\dot{\epsilon}_{ij}}\;dV \;\stackrel{!}{=}\; \text{Min.} \tag{19}$$

Instead of this it is convenient to minimize the ratio of nominal longitudinal stress σ_z and yield strength k_f (A cross section area, r_i inner radius, r_a outer radius)

$$\frac{\sigma_z}{k_f} = \frac{F}{A\,k_f} = \frac{L}{v\,A\,k_f} = \frac{L}{v\,\pi\,(r_a^2 - r_i^2)\,k_f} \;\stackrel{!}{=}\; \text{Min.} \tag{20}$$

or finally

$$\frac{\sigma_z}{k_f} = \sqrt{\tfrac{2}{3}}\,\frac{p+1}{p}\,\frac{1}{\ell\,(r_a^2 - r_i^2)}\int_0^{\ell}\int_{r_i}^{r_a} r\left\{2\left[3+\left(\frac{r_n}{r}\right)^4\right]\left[1-\left(\frac{z}{\ell}\right)^p\right]^2 + \right.$$
$$\left. + \frac{p^2 r^2}{2\ell^2}\left[1-\left(\frac{r_n}{r}\right)^2\right]^2\left(\frac{z}{\ell}\right)^{2p-2}\right\}^{1/2} dr\,dz \;\stackrel{!}{=}\; \text{Min.} \tag{21}$$

The evaluation of this integral and the optimization of the two free parameters r_n and p were done numerically by a two-dimensional Newton method. The following ranges were chosen

$$0 \le r_n \le r_a\,, \qquad 1 \le p \le 5\,. \tag{22}$$

The geometry of the cup was varied as follows

$$\begin{aligned} &r_i / r_a = 0.1 \;\ldots\; (0.1) \;\ldots\; 0.9 \\ &2\,\ell / (r_a - r_i) = 0.5,\ 1,\ 2,\ 4,\ 8,\ 16\,. \end{aligned} \tag{23}$$

Fig. 2 shows the optimized tension stress in dependence on the cup geometry. The longer and the thicker the wall is, the more the tension stress approaches the yield strength in tension. For practicable dimensions r_i = 9 mm, r_a = 11 mm and 2ℓ = 15 mm σ_z is only 13% higher than k_f. As this is an upper bound solution, it is justified to take the measured longitudinal stress as a direct measure for the yield strength in tension.

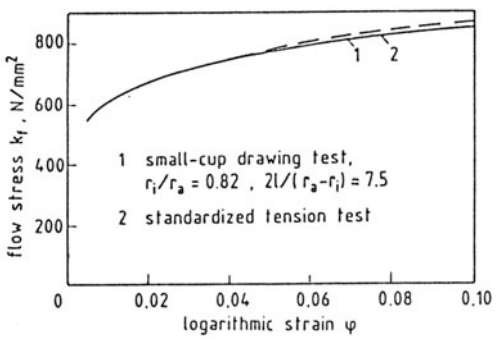

Fig. 3: Comparison of flow curves of steel 20 MnMoNi 5 5, measured by small-cup drawing test and standardized tension test

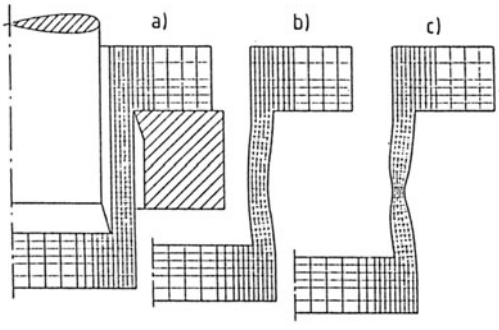

Fig. 4: FEM-calculation of the plastic deformation of a cup with r_i/r_a = 0.82 and $2\ell/(r_a-r_i)$ = 5.71; a) before deformation, b) after 10%, c) after 20% elongation of the wall

Fig. 3 confirms this result by a comparison of flow curves measured by the small-cup drawing test and the standardized tension test [1].

To back up these results by another method, calculations with the finite element method (FEM) were carried out by use of the program FINEL (developed at IBF, Aachen), based on a rigid ideally plastic material and sticking friction at the contact areas. The elements were 4-knot isoparametrical elements. Fig. 4 as an example shows the mode of deformation for 10 and 20% elongation of the wall. The wall is curved inwards, just as it is predicted by the upper bound solution. This curvature was also stated experimentally, Fig. 5 [1].

Concluding the analysis of the small-cup drawing test it should be pointed to the findings that the elongation at fracture in cup drawing is nearly the same as in standardized tension but that the reduction of area by necking is distinctly smaller [1]. An explanation by the theory of plasticity is difficult. A further discussion is, therefore, omitted here.

3 Mantle Compression Test

The cylinder upsetting test is a well-known method for the determination of flow curves. A special development of it is the mantle compression test, Fig. 6. The specimen consists of a cylindrical core, surrounded by a hollow-cylindrical mantle. In gen-

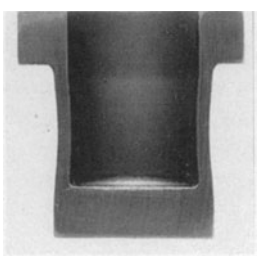

a)

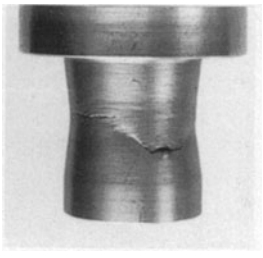

b)

Fig. 5: Deformed cups of steel 20 MnMoNi 5 5; a) at maximum of load, b) after formation of cracks

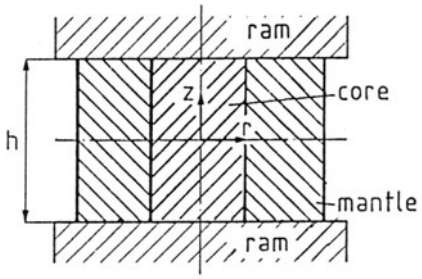

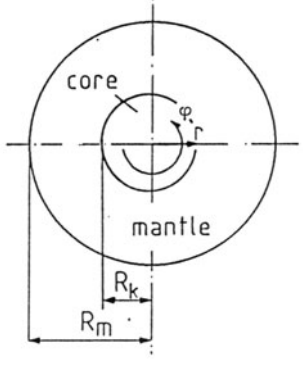

Fig. 6: Principle of the mantle compression test

eral the core is made from the material to be tested, often brittle material, whereas the material of the mantle is softer and more ductile. In case of sticking friction between ram and specimen, i.e. working without a lubricant, the high surface shear stresses cause radial compression stresses in the interface between core and mantle. The core material is, therefore, deformed by axial compression superimposed by a hydrostatic state of stress, which can be controlled by the geometry of the specimen and the amount of plastic deformation. Due to this effect the mantle compression test is mainly used for the investigation of the influence of hydrostatic pressure on ductility. More difficult is the determination of the flow curve of the core material, as the force acting on the core is generally much smaller than that on the mantle. The calculation of the distribution of these two forces from the measured total force can lead to a significant error.

In order to get an impression on the attainable amount of hydrostatic pressure a stress analysis was made on the basis of elementary plastomechanics. Using the well-known tube model due to H. Lippmann [2, 3] the equilibrium of forces and the yield criterion lead to a linear distribution of radial stresses if sticking friction is assumed on the whole contact area. With pressures considered being positive, Fig. 7 demonstrates the distribution of axial pressures σ_z and radial pressures σ_r across the diameter of a mantle compression specimen. At the interface between core and mantle σ_r must be continuous, whereas σ_z shows a jump, as the yield stresses of core and mantle are different. Usually the core is the harder part.

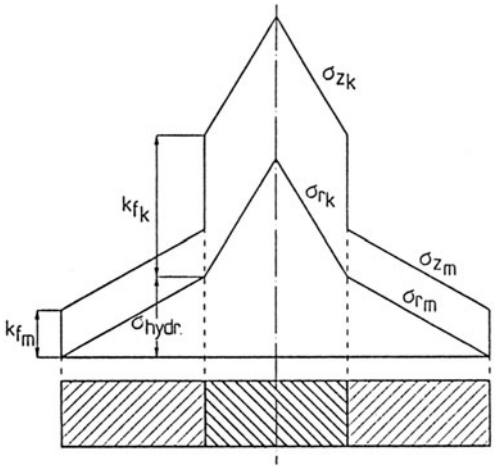

Fig. 7: Pressure distribution in the mantle compression test in case of hard core and soft mantle

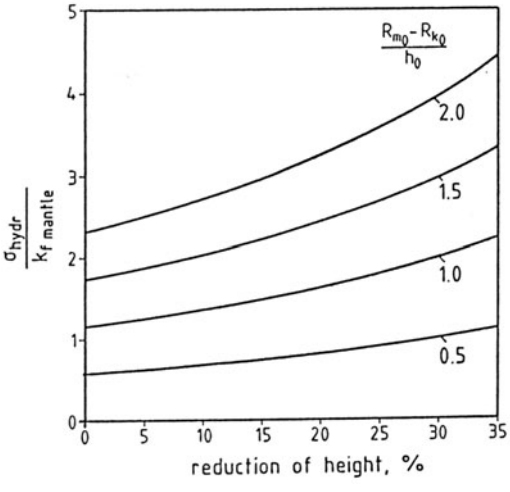

Fig. 8: Hydrostatic pressure in the mantle compression test in dependence on specimen geometry and deformation

The hydrostatic pressure σ_{hydr} equals σ_r at the interface

$$\sigma_{hydr} = \frac{2m_m k_{f_m}}{h_0 \sqrt{3}} (R_{m_0} - R_{k_0}) (1 - \epsilon)^{-3/2} \tag{24}$$

(m friction factor, k_f yield strength, R outer radius, h height, ϵ reduction of height, index k for core, index m for mantle, index 0 for undeformed dimensions). Fig. 8 shows that σ_{hydr} increases with the reduction of height and the ratio of mantle thickness and height. It can be a significant multiple of the yield strength of the mantle material, effecting a large rise of ductility of the core material.

The elementary plastostatic analysis gives the following equation for the axial compression force

$$F = F_k + F_m = \pi \left[k_{f_k} R_k^2 + k_{f_m} (R_m^2 - R_k^2) \right] + \\ + \frac{2\pi}{3h\sqrt{3}} \left[k_{f_k} m_k R_k^3 + k_{f_m} m_m (R_m^3 - R_k^3) \right]. \tag{25}$$

A more detailed insight into the flow of material was again facilitated by use of the upper bound method. In case of homogeneous deformation the constancy of volume would result in the radial velocity (v speed of the ram)

$$v_r = \frac{rv}{2h}. \tag{26}$$

Because of friction the real v_r is smaller at the contact area, which is taken into account by introducing a slide parameter M

$$v_r = \frac{rv}{2h}(1 - M) \quad \text{at} \quad z = \tfrac{1}{2}h. \tag{27}$$

M = 0 means homogeneous deformation, M = 1 means complete sticking.

By use of eq. (27) as a boundary condition the following kinematically admissible velocity field was derived both for core and mantle

$$\begin{aligned} v_r &= \frac{Mrv}{2bh}(b+1)\left[\frac{b+M}{M(b+1)} - \left(\frac{2z}{h}\right)^b\right], \\ v_\varphi &= 0, \\ v_z &= \frac{Mv}{2b}\left[\left(\frac{2z}{h}\right)^{b+1} - \frac{b+M}{M}\left(\frac{2z}{h}\right)\right]. \end{aligned} \tag{28}$$

Besides M a second adaptable parameter b is used therein which describes the bulging of the deformed contour. Additional integrations lead to an equation for the deformed contour of a cylinder area with the initial dimensions $r = R_0$ and $h = h_0$:

$$r = R_0\left(\frac{h_0}{h}\right)^{\frac{b+M}{2b}}\left\{\left(\frac{2z}{h}\right)^b\left[\left(\frac{h_0}{h}\right)^M - 1\right] + 1\right\}^{-\frac{b+1}{2b}}. \tag{29}$$

This equation is also valid for core and mantle if R_0 is replaced by R_{k0} or R_{m0}, respectively.

Fig. 9 shows some examples of deformed contours in dependence on the parameters M and b. Similar to the procedure described for the small-cup drawing test the sum of deformation and friction power was minimized to find the optimal parameters. In case of missing lubrication it is justified to set M = 1. Then the bulging parameter was found to be $b \approx 5$.

The mantle compression test has proved to be an effective method for studying the enhancement of ductility of brittle materials by superimposed hydrostatic pressure. Fig. 10 shows a heavily deformed specimen and the microstructure of gray cast iron without observing any crack [4]. Another application is demonstrated in Fig. 11, showing the microstructure of compacted NiAl-powder [5].

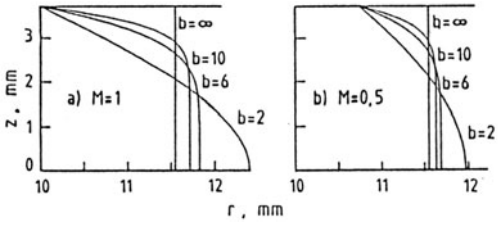

Fig. 9: Calculated contour of a 25% deformed core specimen in dependence on slide parameter M and bulging parameter b; radius before deformation R_0 = 10 mm

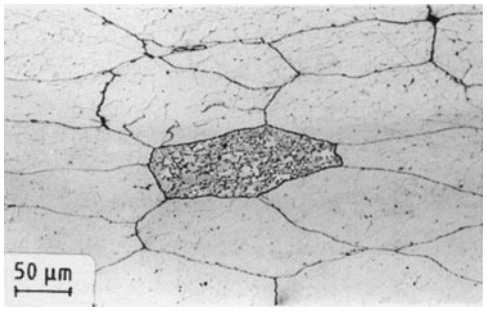

Fig. 11: NiAl-powder, compacted by 50% mantle compression

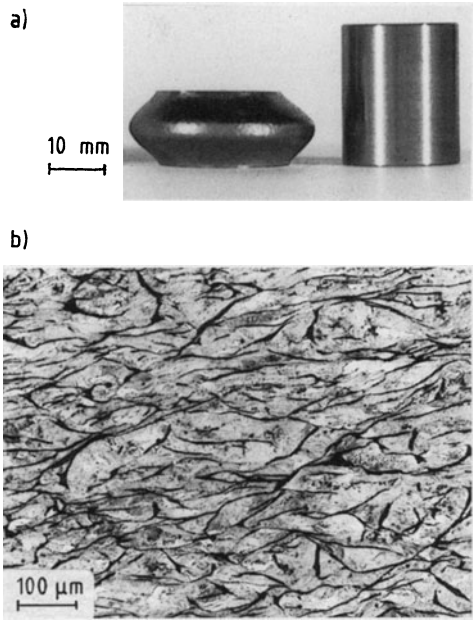

Fig. 10: Core of gray cast iron, 46.7% deformed by mantle compression test; a) change of geometry, b) microstructure

4 Ball Compression Test

In the course of development of a new material sometimes the available masses are very small. If, for example, the material is produced by levitation melting only a small ball-shaped specimen is at hand. An interesting question is whether it is possible to deduce numerical values for the yield strength from a plastic compression of the ball specimen.

In order to investigate the stresses and strains in ball compression, some FEM-calculations, mainly by use of TPS 10 (elastic material) and FARM (rigid-plastic material) [6], and supporting laboratory tests were carried out [7].

Starting with point loads in the very beginning of elastic compression the state of stress is very inhomogeneous. Fig. 12 shows that the equivalent stress is concentrated near the two contact points. With increasing load, plastic flow starts at these points.

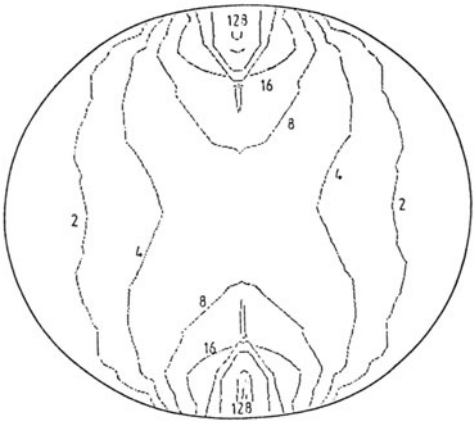

Fig. 12: Isolines of equivalent stress σ_v (N/mm^2) for elastic ball compression (half section in load direction)

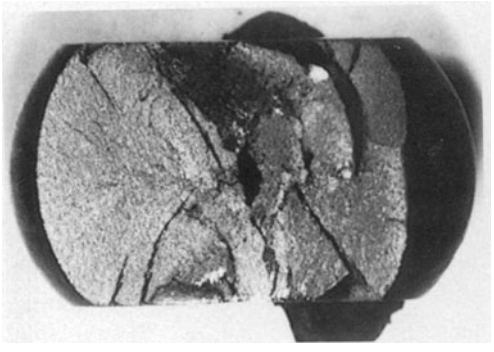

Fig. 14: Fracture of a 15% deformed ball; material 1.2601, hardness 50 HRC, initial diameter 10 mm

Fig. 13 demonstrates the distribution of equivalent strain rate for increased reduction of diameter. Anywhere between 1 and 10% deformation the plastic zone fully extends to the centre of the ball. With increasing flattening of the contacting part of the specimen the deformation in this region is more and more hindered by friction. The highest values of strain rate are therefore to be found in a cross-shaped region of the ball cross section, also very well-known as forging-cross in dieless forging operations.

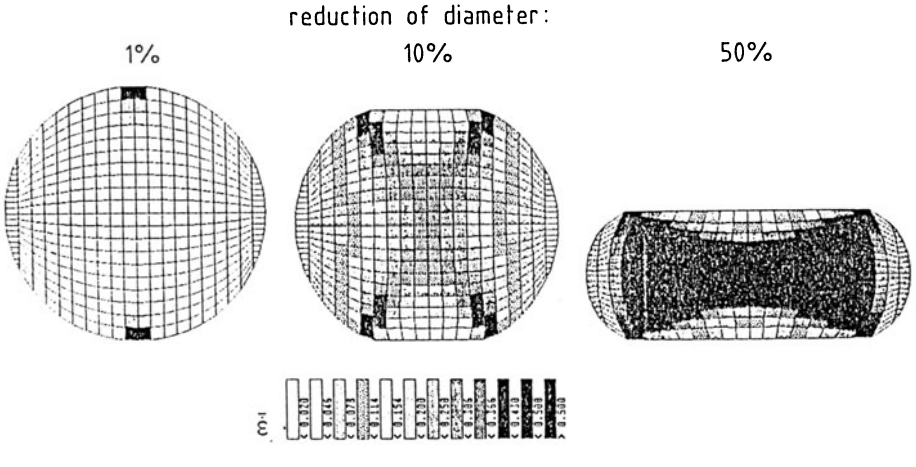

Fig. 13: Distribution of equivalent strain rate in ball compression; steel 30 CrNiMo 8, initial diameter 10 mm, calculated with FARM

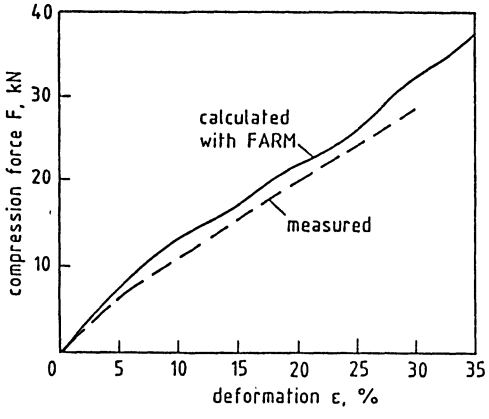

Fig. 15: Comparison of calculated and measured forces in ball compression in dependence on deformation of height; steel C 10, initial diameter 10 mm

This behaviour is confirmed by the type of fracture of the balls, which is often characterized by two internal opposing cones surrounded by the broken outer shell, Fig. 14.

The calculated compression force in dependence on deformation was always higher than the measured one, Fig. 15, what is understandable by the fact that FEM-solutions also belong to the category of upper bound solutions.

At the moment the question, how to determine a flow curve from the ball compression test, cannot be answered satisfactorily.

Acknowledgement

The first author thanks his son, Hartmut O. Pawelski, for the numerical evaluation of equation (21). The authors would like to thank Mr. Günter Deichfischer for the execution of many careful experiments, Dr. Myong-Lae Cho, formerly with IBF, Aachen, for the FEM-calculations, taken as the basis of Fig. 4, and Dipl.-Ing. Martin Eckel for additional calculations. They gratefully acknowledge that a part of the investigation was financially supported by the Deutsche Forschungsgemeinschaft, Bonn.

References

1) Neuhaus, B.: Untersuchung des Einflusses der Probengeometrie von Stahlproben auf die Kenngrößen im Zugversuch. Diplomarbeit, durchgeführt am Max-Planck-Institut für Eisenforschung GmbH in Düsseldorf, Fachhochschule des Landes Rheinland-Pfalz, Abt. Koblenz, 1987.

2) Lippmann, H.: Elementary Methods for the Analysis of Certain Forging Processes. Int. J. Mech. Sci. 1 (1960) S. 109-120.

3) Lippmann, H.: Die elementare Plastizitätstheorie der Umformtechnik. Bänder Bleche Rohre 3 (1962) S. 374-383.

4) Schnorr, W.: Prüfung der Verformbarkeit spröder Werkstoffe. Diplomarbeit, durchgeführt am Max-Planck-Institut für Eisenforschung GmbH in Düsseldorf, Fachhochschule des Landes Rheinland-Pfalz, Abt. Koblenz, 1987.

5) Sembowski, T.: Untersuchung zum Verdichten von Pulver unter Erzeugung eines hydrostatischen Druckes (Pulverschmieden). Diplomarbeit, durchgeführt am Max-Planck-Institut für Eisenforschung GmbH in Düsseldorf, Fachhochschule Bochum, Abt. Gelsenkirchen, 1990.

6) Dung, N. L.: Ein Beitrag zur Berechnung instationärer starr-plastischer Formänderungen mit einer Finite-Element-Methode. Fortschritt-Berichte der VDI-Zeitschriften, Reihe 2 (Betriebstechnik), Nr. 46, Düsseldorf, VDI-Verlag, 1981.

7) Penderok, C.; Schmitt, G.: Theoretische und praktische Untersuchungen zum Kugelstauchen. Diplomarbeit, durchgeführt am Max-Planck-Institut für Eisenforschung GmbH in Düsseldorf, Fachhochschule Iserlohn, Fachbereich Maschinenwesen, 1990.